PIER C

(Received 12 December 2023, Accepted 9 January 2024, Scheduled 22 January 2024)

Design and Analysis of Low Profile Stepped Feedline with Dual Circular Patch MIMO Antenna and Stub Loaded Partial Ground Plane for Wireless Applications

Praveen Kumar[1], Ajit Kumar Singh[2], Ranjeet Kumar[1], Santosh Kumar Mahto[2], Pravesh Pal[1], Rashmi Sinha[1], Arvind Choubey[3], and Ahmed Jamal Abdullah Al-Gburi[4,*]

[1]*Department of Electronics and Communication Engineering, National Institute of Technology Jamshedpur 831014, Jharkhand, India*
[2]*Department of Electronics and Communication Engineering, Indian Institute of Information Technology Ranchi 834010, Jharkhand, India*
[3]*Department of Electronics and Communication Engineering, National Institute of Technology Durgapur 713209, West Bengal, India*
[4]*Center for Telecommunication Research & Innovation (CeTRI), Faculty of Electronics and Computer Technology and Engineering Universiti Teknikal Malaysia Melaka (UTeM), Jalan Hang Tuah Jaya, Durian Tunggal, Melaka 76100, Malaysia*

ABSTRACT: A wideband, dual-element MIMO antenna operating in 2.83–7.21 GHz frequency bands is presented in this study. The proposed design consists of a stub-loaded partial ground plane and a stepped feedline with a dual circle-shaped radiator on top. The designed MIMO antenna operates from 2.83 to 7.21 GHz, covering the C band (4–8 GHz) and 5G (sub-6 GHz) applications. The peak gain observed is 4.8 dBi at 6.2 GHz, with a maximum efficiency of 92% at 3.2 GHz. The minimum port isolation and ECC over the bands 2.83–7.21 are observed as 22 dB and 0.003, respectively. To achieve the best outcome, a parametric analysis of the proposed antenna is also simulated. Various diversity characteristic metrics, including diversity gain (DG), mean effective gain (MEG), total active reflection coefficient (TARC), channel capacity loss (CCL), and ergodic channel capacity (CC), are thoroughly analyzed to determine how well the MIMO antenna performs in terms of diversity. In all operating bands, the measured values provide good agreement with simulation results, indicating a strong candidacy for operation in the investigated bands.

1. INTRODUCTION

Today's communication system has been tremendously changed, which requires fast data rates, low profile, compact portable devices, low power consumption, good isolation, and easy fabrication [1–3]. The implementation of 5G technology in defense, agriculture, healthcare, and the automotive industry holds the potential to bring substantial improvements to the lives of millions of individuals [4, 5]. However, the escalating need for faster data transmission rates is driving a demand for efficient utilization of the electromagnetic spectrum as a resource. Many applications, for reasons related to security and financial considerations, impose constraints on transmitting power levels. In response to these challenges and limitations, wireless engineers have embraced MIMO antenna technology [6, 7], transcending the traditional single-input single-output (SISO) antenna systems. This shift is prompted by the stringent restrictions on available spectrum and power resources.

The deployment of MIMO antenna configurations that were crucial for 4G is anticipated to play a vital role as an enabling system for 5G as well [1]. The communication infrastructure for 5G is expected to support two distinct frequency bands: the sub-6 GHz band and millimeter-wave (mm-wave) band. MIMO systems are essential for increasing data rates in areas with limited bandwidth. The two most important design characteristics of a MIMO system are high isolation and low correlation. Isolation has a negative effect on antenna performance in terms of radiation efficiency. The isolation between the elements is increased by utilizing flawed ground structures and parasitic elements between the radiating elements [8]. With these approaches, it is challenging to provide a wide bandwidth while also offering strong isolation and minimal correlation due to the deterioration of impedance matching. MIMO antennas are used by almost all current 4G-LTE devices, mobile phones, and wireless devices. Several MIMO antennas are suggested in the literature for 5G (sub-6 GHz), WLAN, Wi-Fi, and WiMAX applications.

For applications related to 5G New Radio (NR) sub-6 GHz WLAN, a four-port MIMO antenna system has been introduced [9]. In this configuration, an electromagnetic bandgap is incorporated within the $0.3\lambda_0$ separation between orthogonally oriented antenna elements. Another design discussed in [13] presents a linearly polarized 4×4 MIMO antenna with a bandwidth spanning 1.66–2.17 GHz. At the lower frequency of 1.66 GHz, the suggested antenna exhibits electrical dimensions of $0.38\lambda_0 \times 0.54\lambda_0$ and achieves isolation greater than 12 dB. In the realm of 5.7 GHz wireless applications, [14] proposes a

* Corresponding author: Ahmed Jamal Abdullah Al-Gburi (ahmedjamal@ieee.org) and (ahmedjamal@utem.edu.my).

four-element modified rectangular radiator with multiple cuts and a slightly sloped ground. This antenna achieves mutual coupling exceeding 13 dB and a correlation of 0.04 without the use of a decoupling structure. For 2.4 GHz Wi-Fi applications, [15] recommends a quad-element MIMO antenna featuring a common radiating element. This design focuses on improving port isolation and includes four radiators with partial ground planes and a diagonal parasitic element. The antenna has electrical dimensions measuring $0.56\lambda_0 \times 0.56\lambda_0$, ECC of 0.01, and demonstrates isolation surpassing 13 dB. Another approach outlined in [16] employs a quad-element wideband printed modified monopole-based MIMO antenna system for the same frequency range, utilizing a ground structure with vertical slots and a single circular slot to enhance isolation.

Furthermore, [17] introduced a small, broadband printed directional antenna with a parasitic strip intended for use as an element in a MIMO system. The design incorporated a meander dipole, a concave parabolic reflector, and a parasitic strip for impedance matching. Experimental results indicated that the proposed MIMO array exhibited a wide bandwidth of 23.9% (2.3 to 2.95 GHz).

In [18], a compact MIMO antenna designed for both 4G and 5G applications was introduced, emphasizing high isolation. To achieve wideband characteristics, the design incorporated closed-ended and open-ended rectangular slots on the top plate of each PIFA (Planar Inverted-F Antenna), along with additional slots etched in the ground plane beneath them. Another study, detailed in [19], showcased a small MIMO antenna featuring an embedded network. In order to improve isolation without enlarging the antenna system's footprint, a decoupling network was integrated between the two antennas. Additionally, in [20], a MIMO Half-Shaped Cubical Parasitic Antenna (HSCPA) was presented, providing adjustable frequency and radiation pattern. This antenna utilized PIFA components and employed Schottky diodes for the purpose of reconfiguring frequency and radiation pattern.

For WiFi-LTE applications, [21] recommended a wide-band MIMO antenna system with a 0.6 GHz impedance bandwidth. This proposed antenna comprised two microstrip-fed monopole antennas situated on an L-shaped ground plane. This gave us the idea to create a microstrip dual element MIMO antenna with improved diversity performance, isolation, and return loss in the sub-6 GHz frequency range. An ultra-compact two-port MIMO antenna working in the frequency range of 3.1–10.6 GHz with dual band-notched characteristics was presented [22]. The MIMO antenna consists of two identical octagon-shaped radiating elements placed adjacent to each other with a connected ground plane. A compact modified Sierpinski carpet fractal UWB MIMO antenna with a square-shaped funnel-like ground stub was presented and experimentally investigated [23]. Miniaturization and wideband performance are achieved by using the proposed fractal structure. The dimension of the proposed MIMO antenna is $24 \times 30\,\text{mm}^2$ and consists of two novel modified Sierpinski carpet fractal monopole-antenna elements. A dual-port transparent MIMO antenna resonating at sub-6 GHz 5G band is proposed by using patch/ground material as transparent conductive oxide (AgHT-8) and a transparent Plexiglas substrate [24]. The transparent antennas span over a -10 dB band of 4.65 to 4.97 GHz (300 MHz) with isolation greater than 15 dB between two elements. A compact two-element MIMO antenna with improved isolation for triple-band applications was discussed in [25]. The antenna consists of two radiating elements with a shared ground plane and a novel decoupling structure. Each antenna element has three stubs with different lengths, which work as quarter-wavelength monopoles to give a triple-band operation. The decoupling system was made by etching various slots in an inverted H-shape stub attached to two quarter-circles at its lower ends. The simulated and measured results show that the antenna operates at the key frequency bands of 2.4 GHz (2.29–2.47 GHz), 3.5 GHz (3.34–3.73 GHz), and 5.5 GHz (4.57–6.75 GHz).

In this paper, we introduce a patch of two closely placed circular shapes. A simple rectangular slot with a rectangular stub and thin stub patterns is printed on the ground plane to introduce a defective ground structure, which acts as a resonant stub. These resonant slot and stubs are intended to suppress the surface wave emitted by the adjacent antennas. This leads to enhancing the isolation of the MIMO antenna. The gap between the adjacent antennas is significantly reduced by 4 mm ($0.05\lambda_0$). The maximum isolation of -53 dB at 5.47 GHz is achieved. This MIMO antenna has a compact size $0.44\lambda_0 \times 0.35\lambda_0$ and covers the frequency band from 2.83 to 7.21 GHz, which is appropriate for S-band and a few C-band applications.

The design geometry of proposed work is thoroughly explained in Section 2. The parametric, simulated and experimentally measured MIMO antenna performance parameters are discussed and analyzed in Sections 3 and 4. Finally, in Section 5, this article is concluded.

2. MIMO ANTENNA DESIGN CONFIGURATION

This section describes how the proposed MIMO antenna is evolved. The single element antenna, further it will be used for MIMO antenna, is shown in Figure 1(a) and corresponding reflection coefficient presented in Figure 1(b). The single radiator achieved the bandwidth from 2.83 to 6.55 GHz. The conceptual design of MIMO antenna layout is depicted in Figure 2. The single layer MIMO antenna built on a lossy and inexpensive FR-4 substrate having dielectric constant = 4.3, tangent loss = 0.025, and thickness of 1.6 mm. Radiating elements, partial ground plane (PGP), and thin stub are made of copper of thickness of 0.035 mm. The design parameters of suggested MIMO antenna are tabulated in Table 1. The prototype of MIMO antenna and experimental setup is presented in Figure 3. HFSS 19.0 has been used in simulation for the designed structure.

Figure 4 presents the reflection and transmission coefficients of evolution steps of the proposed antenna. In step 1, a dual port circular patch with a unite stepped feedline and partial ground plane (PGP) is built on an FR-4 substrate, shown in Figure 4. In step 2, the MIMO antenna contains two circular radiators, a 50 Ω microstrip stepped feedline, and a slot in PGP, and wideband could not be achieved. In step 3, the MIMO antenna contains two circular radiators, a 50 Ω microstrip stepped feedline,

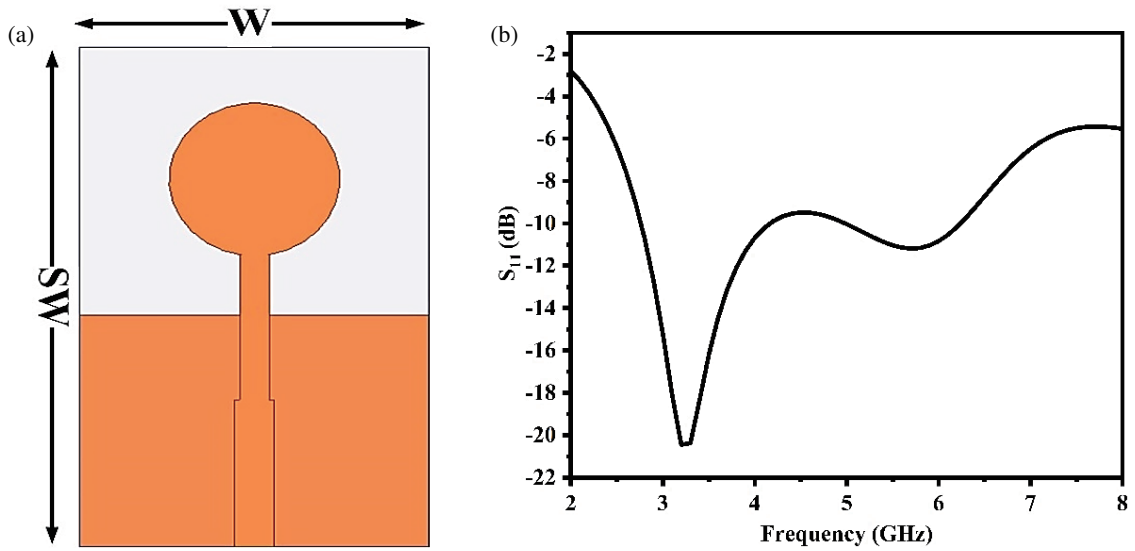

FIGURE 1. (a) Single element radiator. (b) Reflection coefficient.

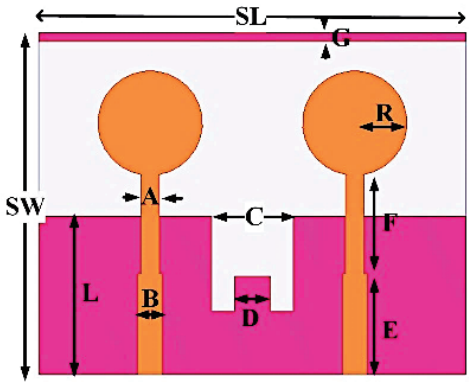

FIGURE 2. Proposed MIMO antenna.

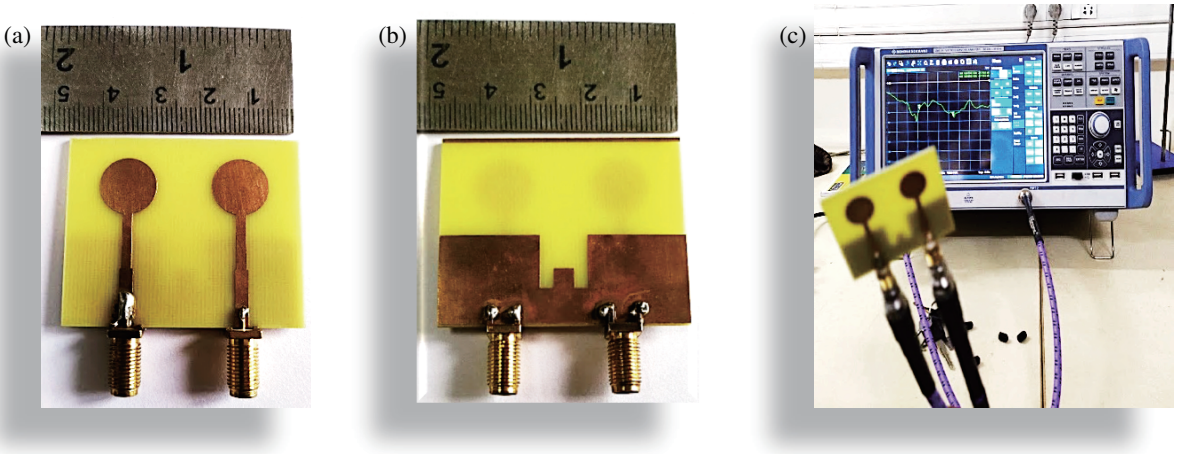

FIGURE 3. The antenna that was designed and constructed is depicted in the following ways: (a) a top view, (b) a bottom view, and (c) an illustration of the experimental setup for the antenna.

a slot, and a rectangular stub within the slot is introduce in PGP. Further in the final step, the proposed antenna contains two circular radiators, a 50 Ω microstrip stepped feedline, PGP, and a rectangular stub is placed in front of the PGP as presented in Figure 4. While loading a stub on PGP, isolation is achieved

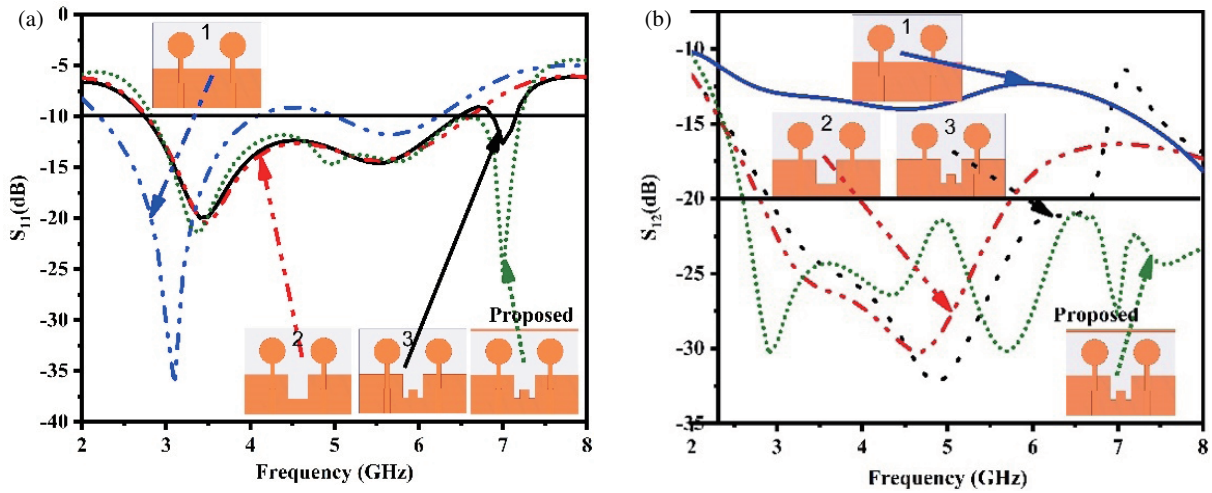

FIGURE 4. Evolution steps of the suggested antenna (a) S_{11} and (b) S_{12}.

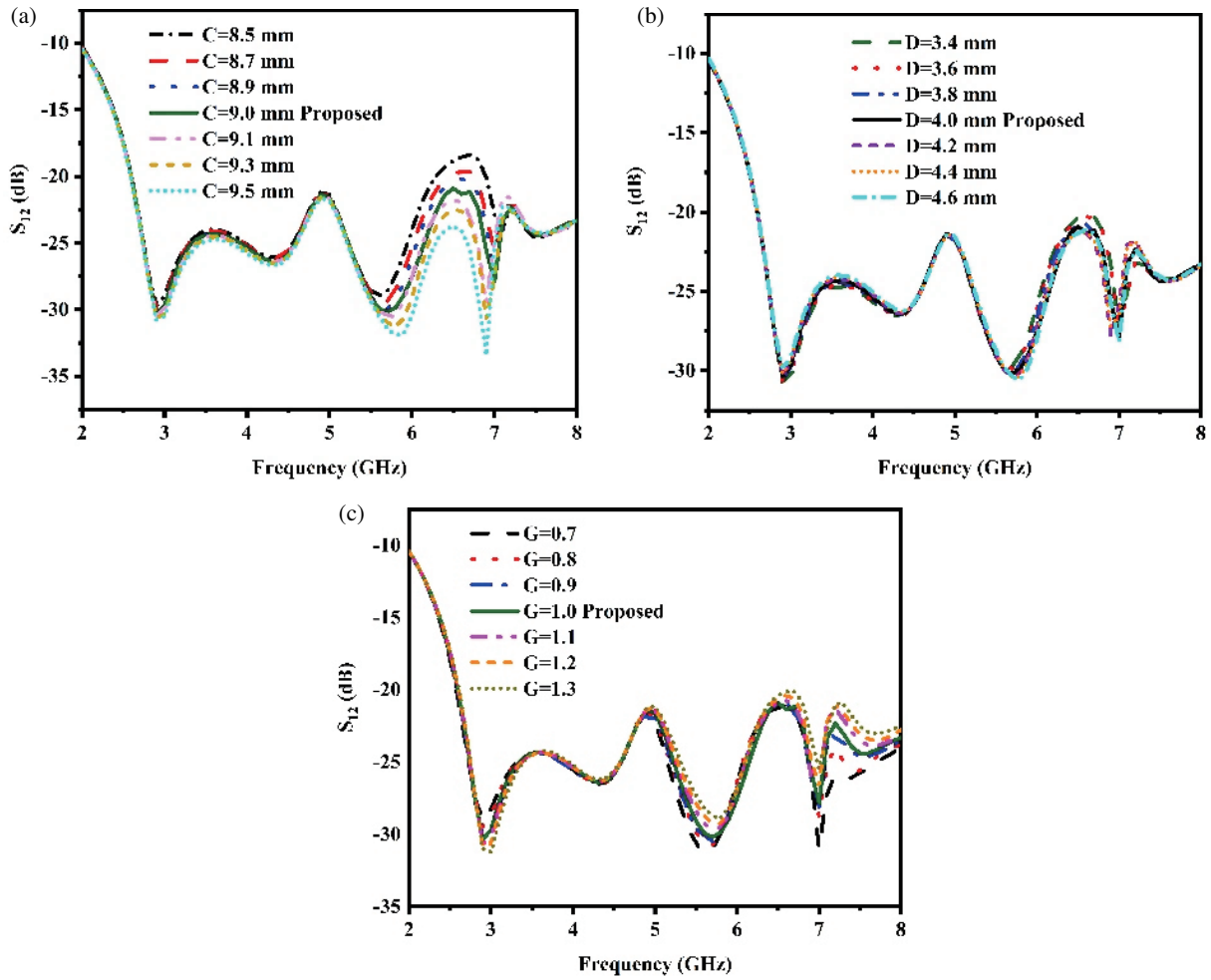

FIGURE 5. Parametric analysis of the proposed MIMO antenna.

up to more than 20 dB throughout the band as shown in Figure 4(b).

Different types of parametric analysis are considered for all presented structures to identify optimum performance. Figure 5 illustrates the outcome of the modifications of parameters C, D, and G on the S_{12} curve. Varying C from 8.5 to 9.5 mm, optimum result is obtained at $C = 9$ mm as shown in Figure 5(a). Further varying D from 3.4 to 4.6 mm, optimum isolation is obtained at $D = 4$ mm as shown Figure 5(b). Up to $G = 1.1$ mm, the isolation rises as G rises; after that point, a change in G re-

TABLE 1. Optimized design parameters (mm).

SL	47.7	**A**	2	**R**	6
SW	38	**B**	2.7	**G**	1
R	6	**C**	9	**E**	11.2
L	17.6	**D**	4	**F**	11

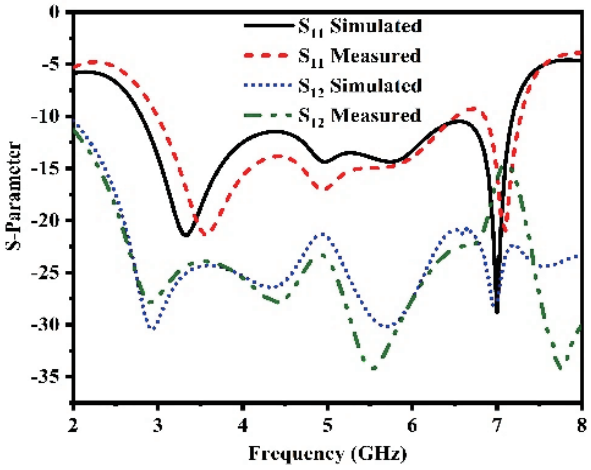

FIGURE 6. Scattering parameter of the suggested design.

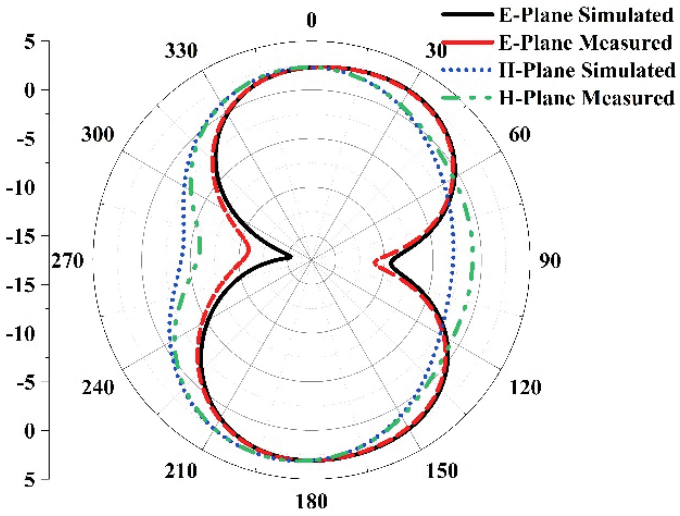

FIGURE 7. 2D-Radiation pattern at 3.5 GHz of the proposed design.

sults in a fall in isolation. Maximum isolation is attained when G is equal to 1 mm. Figure 5(c) shows the effect of the modification to G on isolation.

3. RESULTS AND DISCUSSIONS MIMO ANTENNA

This section presents the analysis of scattering parameters of the proposed design. Because they provide a quantitative evaluation of the antenna's performance, antenna scattering parameters are important in the design and research of antennas. By evaluating the S-parameters, engineers may evaluate the antenna's impedance, radiation pattern, and other elements that affect its ability to transmit and receive information. The measured S_{11} is achieved from 2.98–7.25 GHz, while isolation ranges 16–34 dB. The maximum return loss is obtained at 7 GHz as 30 dB, whereas isolation achieves 16 dB as shown in Figure 6.

The experimental and simulated 2D radiation patterns at 3.5 GHz are shown in Figure 7. Over the whole bandwidth, this pattern remains constant and is unaffected by the negative side-effects of reciprocal coupling. Figure 7 demonstrates that the E-plane has a dumbbell shape (dipole) and that the H-plane is almost omnidirectional.

Figure 8 illustrates the total efficiency and gain of the MIMO antenna. The simulated average efficiency and measured gain

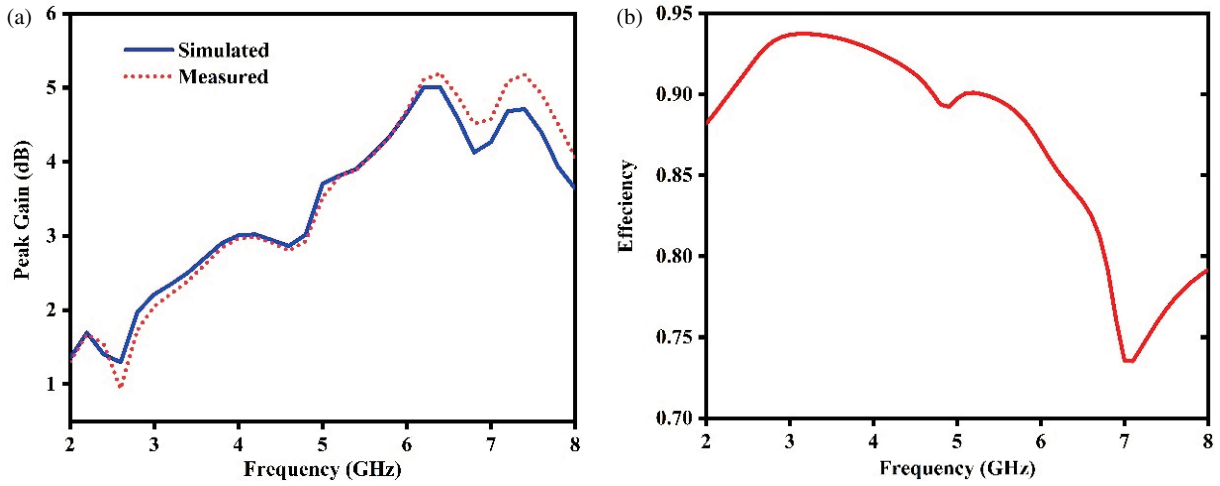

FIGURE 8. (a) Peak gain. (b) Radiation Efficiency.

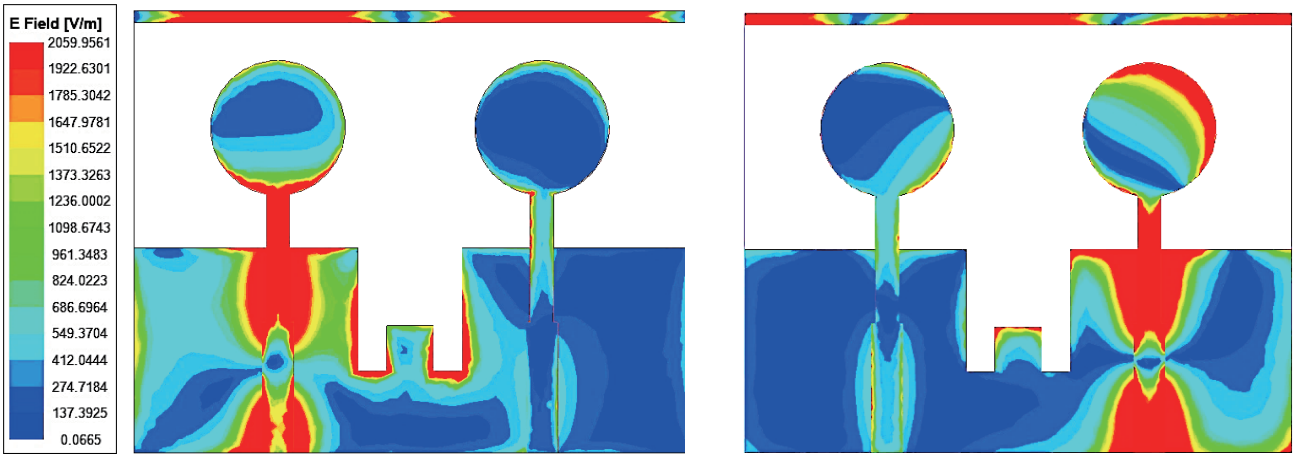

FIGURE 9. MIMO antenna surface current density at 3.5 GHz.

of the antenna across different frequency bands are observed to be in the ranges of 73–92% and 1.6–4.7 dBi, respectively. Figure 9 at 3.5 GHz shows the surface current density that is present on the antenna construction. When port 1 (Ant-1(left)) is triggered and port 2 (Ant-2(right)) matched by a 50 Ω load, surface waves are seen in Figure 9. Another powerful surface wave is produced on the left border of the parasitic strip and the slot. Due to the high mutual coupling (MC), it can be concluded that the MIMO antenna requires the suggested decoupling strategy in order to function without interference from nearby antennas.

4. DIVERSITY PERFORMANCE PARAMETERS

When multiple antenna components are employed, the Envelope Correlation Coefficient (ECC) offers a means to quantify the correlation degree of their respective signal envelopes. The signal's envelope, in this context, pertains to its magnitude without considering its phase. ECC is a statistical measure assessing the similarity of signal envelopes received by different antennas. The spatial diversity gain achievable with multiple antennas diminishes when ECC approaches 1, indicating the strong coupling between signals received by various antennas. Conversely, a small ECC suggests independent signals received by different antennas, allowing for maximum spatial diversity gain. ECC is derived from power levels and the correlation coefficient between signals received by different antenna components. Techniques such as cross-correlation and autocorrelation are employed to determine the correlation coefficient, providing a linear measure of the relationship between signals received by different antennas. Factors like antenna coupling, mutual coupling, reflections, and scattering from surrounding objects can contribute to an increased ECC. If these factors result in undesirable correlations among signals received by different antennas, the spatial diversity gain achievable by the MIMO system may be compromised. Equation (1) is used to calculate ECC.

$$\mathrm{ECC} = \frac{\left|S_{11}^{*}S_{12} + S_{21}^{*}S_{22}\right|^{2}}{\left(1-\left|S_{11}\right|^{2}-\left|S_{21}\right|^{2}\right)\left(1-\left|S_{22}\right|^{2}-\left|S_{12}\right|^{2}\right)} \quad (1)$$

$$\mathrm{ECC} = \rho_{i,j} = \frac{\left|\iint_{4\pi}\left[\vec{M}_i(\theta,\varphi)\cdot\vec{M}_j(\theta,\varphi)\right]d\Omega\right|^{2}}{\left[\iint_{4\pi}\left|\vec{M}_i(\theta,\varphi)\right|^{2}d\Omega\right]\cdot\left[\iint_{4\pi}\left|\vec{M}_j(\theta,\varphi)\right|^{2}d\Omega\right]} \quad (2)$$

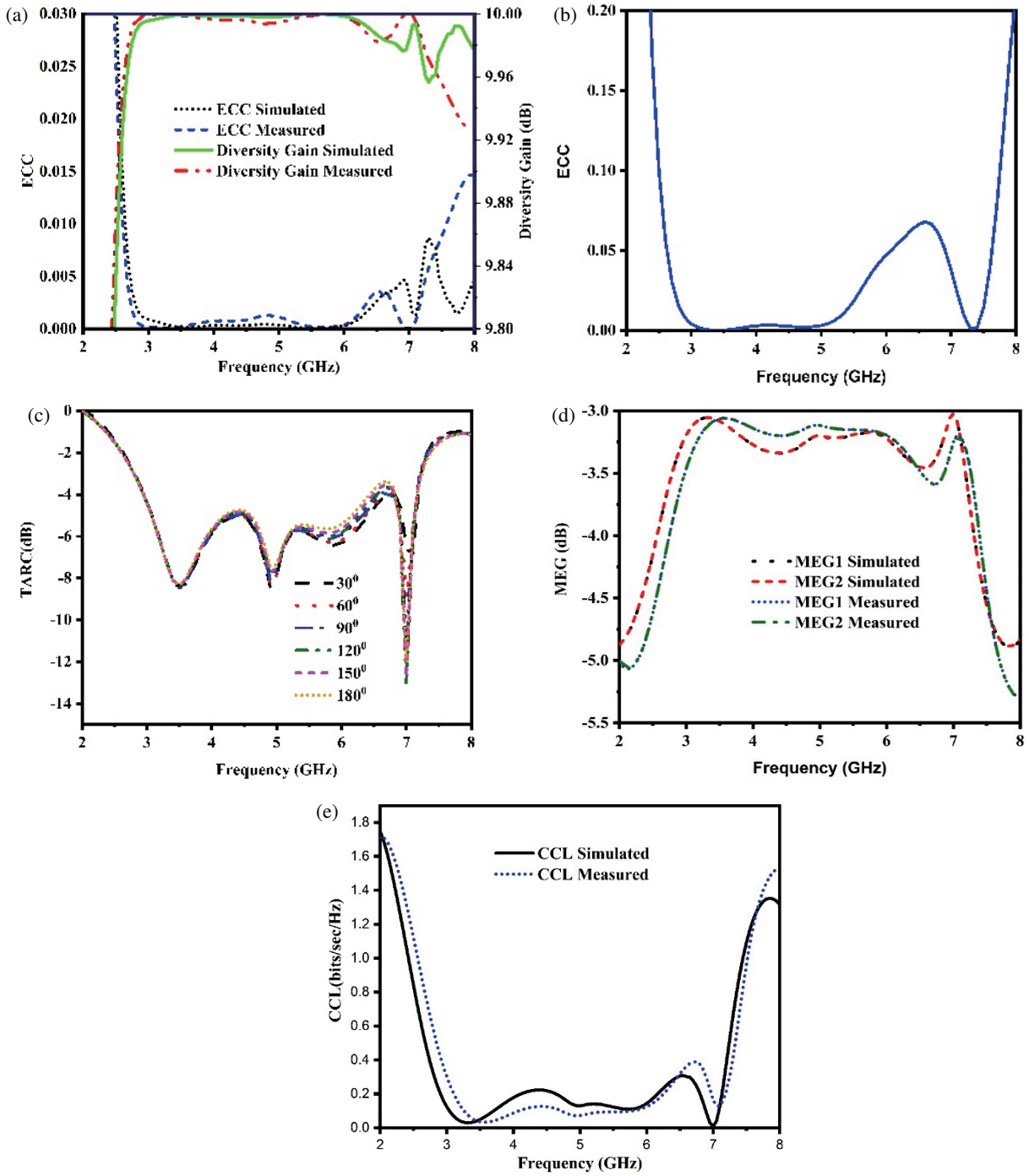

FIGURE 10. (a) ECC & DG through S-Parameter. (b) ECC through far field method. (c) TARC. (d) MEG. (e) CCL.

In this scenario, '$\vec{M}_i\,(\theta,\varphi)$' signifies the three-dimensional radiation pattern observed when antenna 'i' is activated, while another occurrence of '$\vec{M}_j\,(\theta,\varphi)$' is indicative of the three-dimensional radiation pattern when antenna 'j' is activated. The solid angle in this context is denoted by the symbol Ω. The effectiveness of the MIMO system is quantified by the diversity gain (DG). The calculation of diversity gain is facilitated by ECC, which can be computed using Equation (2) [19].

$$\mathrm{DG}_{i,j} = 10\sqrt{1-\mathrm{ECC}_{i,j}^2} \tag{3}$$

Total Active Reflection Coefficient (TARC) is defined as the square root of the total reflected power divided by the total incident power. TARC serves as a reliable indicator of MIMO antenna efficiency as it incorporates information about the impact of mutual coupling. The calculation of TARC for an N-unit MIMO antenna configuration can be carried out utilizing formula (4) [19].

$$\mathrm{TARC} = N^{-0.5}\sqrt{\sum_{i=1}^{N}\left|\sum_{K=1}^{N} S_{ik}e^{j\theta_{k-1}}\right|^2} \tag{4}$$

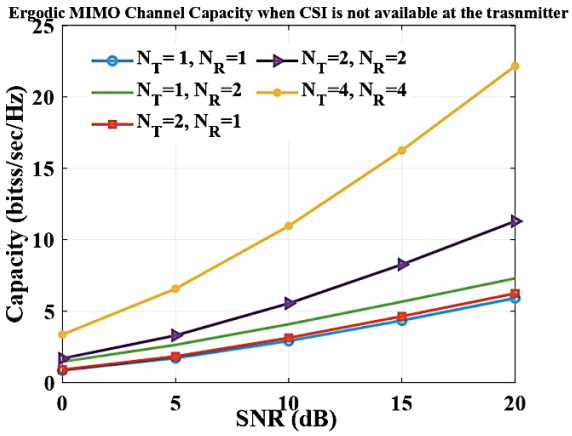

FIGURE 11. Channel capacity.

TARC is expected to range from 0 to 1, with the ideal TARC value being less than 0 dB, as depicted in Figure 10(b). Another critical metric for assessing MIMO diversity performance is the Mean Effective Gain (MEG), which compares the power received by the isotropic antenna to the power acquired by the diversity antenna in a fading environment. The MEG for the i^{th} element of the MIMO system can be calculated using Equation (5) [20, 26], and the results are illustrated in Figure 10(c).

$$\text{MEG}_i = 0.5\left[1 - \sum_{n=1}^{N} |S_{in}|^2\right] \tag{5}$$

In this context, "N" represents the quantity of elements in the MIMO (Multiple Input, Multiple Output) system.

Another essential metric for evaluating MIMO performance is the Channel Capacity Loss (CCL), which signifies the maximum data delivery rate without encountering substantial losses. The computation of CCL can be accomplished using Equation (5) [20]. For optimal MIMO antenna performance, it is recommended that CCL remains below 0.4 bps/Hz across the entire operating frequency spectrum. In this study, the highest CCL value, obtained through both simulation and measurement, is below 0.3 bps/Hz across various frequency ranges, indicating a robust suitability for the intended band. Figure 10(d) illustrates a plot of CCL versus frequency.

$$\text{CCL} = -\log_2\left[det\left(\varphi^R\right)\right] \tag{6}$$

$$\text{where} \quad \varphi^R = \begin{pmatrix} \alpha 11 & \alpha 12 & \cdots & \alpha 1N \\ \alpha 21 & \alpha 22 & \cdots & \alpha 2N \\ \vdots & \vdots & \vdots & \vdots \\ \alpha N1 & \alpha N2 & \cdots & \alpha NN \end{pmatrix},$$

$$\left(\alpha ii = 1 - \left(\left|\sum_{j=1}^{j=N} S_{ij}^* S_{ji}\right|\right)\right),$$

$$\left(\alpha ik = -\left|\sum_{j=1}^{j=N} S_{ij}^* S_{jk}\right|\right),$$

$$1 \le i \le N, 1 \le k \le N \text{ and } N = 4$$

The ergodic channel capacity (CC), calculated under the assumption of no Envelope Correlation Coefficient (ECC) among the transmitting antennas, serves as a highly effective metric for assessing diversity characteristics in a MIMO system. Equation (7) is employed to assess the channel matrix "H" for this purpose.

$$H = \sqrt{\rho_{scale,RX}} H_{iid} \sqrt{\rho_{scale,TX}} \tag{7}$$

In this context, matrix H_{iid} is a 4×4 matrix with elements comprising independent and identically distributed complex Gaussian random variables. Matrix $\rho_{scale,TX}$, a 2×2 matrix calculated at the transmitter end, is derived under the assumption of null ECC and 100 percent efficiency. On the other hand, another matrix $\rho_{scale,RX}$ is computed as a 2×2 matrix, taking into account the measured ECC and efficiency, as detailed in the explanations provided in references [21, 24].

Further $\rho_{\text{scale,RX}}$ is calculated using Equation (8).

$$\rho_{scale,RX} = \sqrt{n_{total}} \rho_{RX} \sqrt{n_{total}} \tag{8}$$

Equation (8) employs the variables ρ_{RX} and n_{total}, representing the efficiencies of receiving antennas, specifically ECC (envelope correlation coefficient), and total efficiency, respectively. To calculate the ergodic channel capacity denoted as C, the estimation relies on the utilization of Equation (9) as outlined in [22].

$$C = E\left\{\log_2\left[det\left(I + \frac{SNR}{n_T} HH^H\right)\right]\right\} \tag{9}$$

In Equation (9), the variables H^H, SNR, n_T, E, and I represent the Hermitian transpose, signal-to-noise ratio, the number of antennas at the transmitter side, bandwidth, and Identity matrix, respectively. The expectation is taken with respect to different channel realizations, and the variable 4×4 identity matrix is denoted as '4×4 I'. For 4×4 MIMO and 2×2 MIMO, the respective ideal channel capacities (CCs) are 22.2 bps/Hz and 11.3 bps/Hz at an SNR of 20 dB. It is recommended that the CC should be at least 60% of the ideal value for optimal performance of a MIMO antenna, as indicated in [23, 25]. The simulated CC over the operating frequency bands is reported to

TABLE 2. Comparison table of recent reported articles.

Ref.	Electrical Size (mm^2)	Absolute size (mm^2)	No. of ports	Frequency range (GHz)	Fractional bandwidth (FBW) (%)	BDR	Isolation (dB)	ECC
[15]	$0.47\lambda_0 \times 0.47\lambda_0$	$50 \times 100 = 5000$	2	2–3.6	57.14	258.66	20	0.21
[16]	$0.49\lambda_0 \times 0.49\lambda_0$	$50 \times 50 = 2500$	2	3.4–3.6	5.7	23.74	20	0.02
[17]	$1.12\lambda_0 \times 1.12\lambda_0$	$120 \times 60 = 7200$	2	4–14	111	88.48	15	0.1
[18]	$0.8\lambda_0 \times 0.96\lambda_0$	$230 \times 18.5 = 4255$	2	2.3–2.9	23.07	300.39	15	0.15
[23]	$0.76\lambda_0 \times 0.96\lambda_0$	$24 \times 30 = 720$	2	3–12.6	123.07	168.68	26	0.05
[24]	$0.8\lambda_0 \times 0.56\lambda_0$	$50 \times 40 = 2000$	2	4.65–4.97	6.65	14.84	15	0.03
[25]	$0.51\lambda_0 \times 0.36\lambda_0$	$44 \times 35 = 1540$	2	2.28–2.47 3.34–3.73 4.57–6.75	8.0 11.01 38.5	43.57 59.96 209.69	20	0.003
[30]	$1.3\lambda_0 \times 1.0\lambda_0$	$45 \times 45 = 2025$	2	4.85–5.05	4.04	3.10	10	-
[31]	$0.167\lambda_0 \times 0.17\lambda_0$	$43 \times 43 = 1849$	2	2.27–2.35	3.46	121.87	20	-
This work	$\mathbf{0.44\lambda_0 \times 0.35\lambda_0}$	$\mathbf{47.7 \times 38 = 1812.6}$	**2**	**2.83–7.21**	**87.25**	566.55	**22**	**0.003**

be 10.62 bits/sec./Hz. The channel capacity versus frequency is illustrated in Figure 11.

Table 2 shows the comparative table with previous published articles. The proposed antenna achieved a fractional bandwidth of 87.25%, which is better than the other published literature. The ECC and isolation proposed is 0.003 and 22 dB respectively, which is better than [15–18, 24, 25, 30, 31], however less than [9, 23].

Bandwidth dimension ratio (BDR), which is an important parameter to assure properties and compactness of proposed antenna, is given by:

$$\text{BDR} = \frac{\text{BW\%}}{\lambda_0\text{length} \times \lambda_0\text{width}} \tag{10}$$

in which BW represents the bandwidth, and λ_0 length and λ_0 width are the length and width of the antenna individually regarding a frequency relating to the lower cutoff frequency.

5. CONCLUSION

The proposed design operates on three widebands, covering the frequency range of 2.83–7.21 GHz for various wireless applications. Analysis of the antenna's diversity performance considers parameters such as diversity gain, average efficiency, total interference ratio, and channel capacity loss. Across the entire frequency range (2.83–7.21 GHz), both the MEG and TARC consistently register values below 0.2 dB and -5 dB, respectively. Additionally, the channel capacity loss (CCL) remains below 0.3 bps/Hz in all operating bands. Notably, the measured values closely correspond to the simulation results, affirming the antenna's suitability for effective operation across the investigated frequency bands.

ACKNOWLEDGEMENT

The authors express their gratitude for the support received from Universiti Teknikal Malaysia Melaka (UTeM) and the Ministry of Higher Education of Malaysia (MOHE).

REFERENCES

[1] "5G: A technology vision," White Paper, Huawei Technologies Co and Ltd., 2013.

[2] Elabd, R. H. and A. J. A. Al-Gburi, "Super-compact 28/38 GHz 4-port MIMO antenna using metamaterial-inspired EBG structure with SAR analysis for 5G cellular devices," *Journal of Infrared, Millimeter, and Terahertz Waves*, 1–31, 2023.

[3] "5G network architecture: A high-level perspective," Huawei Technologies Co and Ltd., 2017.

[4] Saeidi, T., A. J. A. Al-Gburi, and S. Karamzadeh, "A miniaturized full-ground dual-band MIMO spiral button wearable antenna for 5G and sub-6 GHz communications," *Sensors*, Vol. 23, No. 4, 1997, 2023.

[5] Sarkar, D. and K. V. Srivastava, "Four element dual-band sub-6 GHz 5G MIMO antenna using SRR-loaded slot-loops," in *2018 5th IEEE Uttar Pradesh Section International Conference on Electrical, Electronics and Computer Engineering (UPCON)*, 1–5, 2018.

[6] Ali, A., M. E. Munir, M. M. Nasralla, M. A. Esmail, A. J. A. Al-Gburi, and F. A. Bhatti, "Design process of a compact tri-band MIMO antenna with wideband characteristics for sub-6 GHz, Ku-band, and millimeter-wave applications," *Ain Shams Engineering Journal*, Vol. 15, No. 3, 102579, 2024.

[7] Elabd, R. H. and A. J. A. Al-Gburi, "SAR assessment of miniaturized wideband MIMO antenna structure for millimeter wave 5G smartphones," *Microelectronic Engineering*, Vol. 282, 112098, 2023.

[8] Sharawi, M. S., "Current misuses and future prospects for printed multiple-input, multiple-output antenna systems [wireless corner]," *IEEE Antennas and Propagation Magazine*, Vol. 59, No. 2, 162–170, 2017.

[9] Megahed, A. A., M. Abdelazim, E. H. Abdelhay, and H. Y. M. Soliman, "Sub-6 GHz highly isolated wideband MIMO antenna arrays," *IEEE Access*, Vol. 10, 19 875–19 889, Feb. 2022.

[10] Kumar, A., A. Q. Ansari, B. K. Kanaujia, J. Kishor, and L. Matekovits, "A review on different techniques of mutual coupling reduction between elements of any MIMO antenna. Part 1: DGSs and parasitic structures," *Radio Science*, Vol. 56, No. 3, 1–25, Mar. 2021.

[11] Kumar, A., A. Q. Ansari, B. K. Kanaujia, J. Kishor, and L. Matekovits, "A review on different techniques of mutual coupling reduction between elements of any MIMO antenna. Part 1: DGSs and parasitic structures," *Radio Science*, Vol. 56, No. 3, 1–25, Mar. 2021.

[12] Singh, A. K., S. K. Mahto, and R. Sinha, "Compact super-wideband MIMO antenna with improved isolation for wireless communications," *Frequenz*, Vol. 75, No. 9-10, 407–417, 2021.

[13] Ikram, M., R. Hussain, O. Hammi, and M. S. Sharawi, "An l-shaped 4-element monopole MIMO antenna system with enhanced isolation for mobile applications," *Microwave and Optical Technology Letters*, Vol. 58, No. 11, 2587–2591, Nov. 2016.

[14] Ding, K., C. Gao, D. Qu, and Q. Yin, "Compact broadband MIMO antenna with parasitic strip," *IEEE Antennas and Wireless Propagation Letters*, Vol. 16, 2349–2353, Jun. 2017.

[15] Chattha, H. T., "Compact high isolation wideband 4G and 5G multi-input multi-output antenna system for handheld and internet of things applications," *International Journal of RF and Microwave ComputerAided Engineering*, Vol. 29, No. 6, e21710, 2019.

[16] Zhang, X. Y., C.-D. Xue, Y. Cao, and C.-f. Ding, "Compact MIMO antenna with embedded decoupling network," in *2017 IEEE International Conference on Computational Electromagnetics (ICCEM)*, 64–66, IEEE, 2017.

[17] Padmanathan, S., A. A. Al-Hadi, P. J. Soh, and M. F. Jamlos, "Dual port MIMO half-shaped cubical parasitic pifa design for pattern and frequency reconfiguration applied in mobile terminals," in *2016 IEEE Asia-Pacific Conference on Applied Electromagnetics (APACE)*, 136–140, IEEE, 2016.

[18] Moradikordalivand, A., C. Y. Leow, T. A. Rahman, S. Ebrahimi, and T. H. Chua, "Wideband MIMO antenna system with dual polarization for WiFi and LTE applications," *International Journal of Microwave and Wireless Technologies*, Vol. 8, No. 3, 643–650, 2016.

[19] Mahto, S. K., A. K. Singh, R. Sinha, M. Alibakhshikenari, S. Khan, and G. Pau, "High isolated four element MIMO antenna for ISM/LTE/5G (sub-6 GHz) applications," *IEEE Access*, Vol. 11, 82 946–82 959, 2023.

[20] Singh, A. K., S. K. Mahto, P. Kumar, and R. Sinha, "Analysis of path loss and channel capacity in quad element MIMO antenna for terahertz communication systems," *International Journal of Circuit Theory and Applications*, Vol. 51, No. 3, 1460–1475, 2023.

[21] Taheri, M. M. S., A. Abdipour, S. Zhang, and G. F. Pedersen, "Integrated millimeter-wave wideband end-fire 5G beam steerable array and low-frequency 4G LTE antenna in mobile terminals," *IEEE Transactions on Vehicular Technology*, Vol. 68, No. 4, 4042–4046, 2019.

[22] Kumar, A., A. Q. Ansari, B. K. Kanaujia, J. Kishor, and S. Kumar, "An ultra-compact two-port UWB-MIMO antenna with dual band-notched characteristics," *AEU-International Journal of Electronics and Communications*, Vol. 114, 152997, 2020.

[23] Gurjar, R., D. K. Upadhyay, B. K. Kanaujia, and A. Kumar, "A compact modified sierpinski carpet fractal UWB MIMO antenna with square-shaped funnel-like ground stub," *AEU-International Journal of Electronics and Communications*, Vol. 117, 153126, 2020.

[24] Desai, A., M. Palandoken, I. Elfergani, I. Akdag, C. Zebiri, J. Bastos, J. Rodriguez, and R. A. Abd-Alhameed, "Transparent 2-element 5G MIMO antenna for sub-6 GHz applications," *Electronics*, Vol. 11, No. 2, 251, 2022.

[25] Bayarzaya, B., N. Hussain, W. A. Awan, M. A. Sufian, A. Abbas, D. Choi, J. Lee, and N. Kim, "A compact MIMO antenna with improved isolation for ISM, sub-6 GHz, and WLAN application," *Micromachines*, Vol. 13, No. 8, 1355, 2022.

[26] Zou, H., Y. Li, C.-Y.-D. Sim, and G. Yang, "Design of 8×8 dual-band MIMO antenna array for 5G smartphone applications," *International Journal of RF and Microwave Computer-Aided Engineering*, Vol. 28, No. 9, e21420, 2018.

[27] Loyka, S. L., "Channel capacity of MIMO architecture using the exponential correlation matrix," *IEEE Communications Letters*, Vol. 5, No. 9, 369–371, 2001.

[28] Sharma, P., R. N. Tiwari, P. Singh, P. Kumar, and B. K. Kanaujia, "MIMO antennas: Design approaches, techniques and applications," *Sensors*, Vol. 22, No. 20, 7813, 2022.

[29] Yun, J. X. and R. G. Vaughan, "Multiple element antenna efficiency and its impact on diversity and capacity," *IEEE Transactions on Antennas and Propagation*, Vol. 60, No. 2, 529–539, 2012.

[30] Glazunov, A. A., A. F. Molisch, and F. Tufvesson, "Mean effective gain of antennas in a wireless channel," *IET Microwaves, Antennas & Propagation*, Vol. 3, No. 2, 214–227, 2009.

[31] Bait-Suwailam, M. M., O. F. Siddiqui, and O. M. Ramahi, "Mutual coupling reduction between microstrip patch antennas using slotted-complementary split-ring resonators," *IEEE Antennas and Wireless Propagation Letters*, Vol. 9, 876–878, 2010.

[32] Chiu, C.-Y., C.-H. Cheng, R. D. Murch, and C. R. Rowell, "Reduction of mutual coupling between closely-packed antenna elements," *IEEE Transactions on Antennas and Propagation*, Vol. 55, No. 6, 1732–1738, 2007.